



ing mechanism for the CO transition would explain the observation of incommensurate order with wavevector  $\mathbf{q} = (1-x)\mathbf{b}^*$  [9] and may also be relevant to colossal magnetoresistance (CMR) phases of manganites where diffuse satellites in x-ray scattering have been observed [21, 22] and attributed to polarons with transverse displacements of ions [22] similar to those in Fig. 1(a).

Structure optimizations were performed using the CRYSTAL program [23]. A  $\sqrt{2} \times \sqrt{2} \times 2$  unit cell (Fig. 1) containing eight formula units with ferromagnetic (FM) order was used for optimizations while total energies of A and CE-type magnetically ordered structures were compared using  $2\sqrt{2} \times 2\sqrt{2} \times 2$  unit cells. A single force evaluation was carried out for CE-type magnetic order for a structure which had been optimized with FM magnetic order in order to estimate the importance of magnetoelectric effects on the crystal structure; these were found to be small. No simultaneous relaxation of unit cell dimensions was performed as the calculations are expensive in computer time; unit cell dimensions were taken from experiment [2] ( $a = 5.4763 \text{ \AA}$ ,  $b = 10.8932 \text{ \AA}$ ,  $c = 7.5247 \text{ \AA}$ ). Structure optimizations were performed for 60%, 80% and 100% exact exchange (the latter is simply an unrestricted Hartree-Fock (UHF) calculation); both 60% and 80% exact exchange calculations resulted in CB CO for all space groups investigated while 100% exact exchange resulted in ZP CO structures. Initial atomic configurations were taken from Table II in Ref. [2] ( $P112_1/m$  symmetry) or were generated by hand. As noted by Daoud-Aladine and coworkers [14], the isotropy subgroups of the parent high temperature  $Pbnm$  phase that have a doubled unit cell along the  $\mathbf{b}$  axis are:  $P11m$ ,  $P2_1nm$ ,  $P112_1/m$ ,  $P112_1/b$ ,  $P2_1nb$  and  $P11b$ . The relevant isotropy subgroups for ZP CO are  $P2_1nm$  and  $P11m$  and for CB CO they are  $P112_1/m$  [2] and  $P11m$ .

Hessian matrices for energy minimized CB or ZP CO structures with these space groups had at least one negative eigenvalue, which indicates that they are saddle points on the potential energy surface. A further energy minimization was performed using  $P12_11$  symmetry and 100% exact exchange. The screw axis parallel to the  $\mathbf{b}$  axis naturally incorporates transverse Mn displacements found in experiment. All Hessian matrix eigenvalues were positive for this ZP CO structure and it was lower in energy than the other structures ( $P11m +7 \text{ meV/Mn ion}$ ;  $P2_1nm +14 \text{ meV/Mn ion}$ ). A structure optimization with 60% exact exchange and  $Pn2_1m$  symmetry resulted in a stable CB CO structure which was  $31 \text{ meV/Mn ion}$  lower than the optimized structure with  $P112_1/m$  symmetry. Fractional coordinates for the lowest energy CB and ZP CO structures found, which have  $Pn2_1m$  symmetry, are given in Table I. Fractional coordinates for the  $\text{La}_{0.5}\text{Ca}_{0.5}\text{MnO}_3$  ZP CO structure are compared to those determined by neutron scattering for  $\text{Pr}_{0.60}\text{Ca}_{0.40}\text{MnO}_3$  [14] in Table II.

Fig. 1(a) shows atomic positions for nearly coplanar

TABLE I: Fractional coordinates for  $\text{La}_{0.5}\text{Ca}_{0.5}\text{MnO}_3$  with  $Pn2_1m$  symmetry from *ab initio* total energy minimization. Wyckoff positions are given in the second column. Coordinates on the left were determined using 100% exact exchange and those on the right using 60% exact exchange. Both structures have the (x,y) coordinates of the Mn1 ion in common.

Atom	Wyck.	100%			60%		
		x	y	z	x	y	z
Ca1	2a	0.4773	0.8866	0.0000	0.4861	0.8866	0.0000
La2	2a	0.4652	0.3732	0.0000	0.4514	0.3673	0.0000
La3	2a	0.9760	0.1226	0.5000	0.9743	0.1261	0.5000
Ca4	2a	0.9789	0.5985	0.5000	0.9779	0.6057	0.5000
Mn1	4b	0.0000	0.8746	0.2445	0.0000	0.8713	0.2478
Mn2	4b	0.4578	0.6224	0.2534	0.4811	0.6231	0.2535
O1	4b	0.2463	0.0069	0.2109	0.2352	0.9977	0.2109
O2	4b	0.2556	0.7600	0.2112	0.2676	0.7600	0.2144
O3	4b	0.1813	0.2315	0.2042	0.2118	0.2433	0.2146
O4	4b	0.7479	0.9891	0.2753	0.7539	0.9970	0.2717
O1'	2a	0.4298	0.1255	0.5000	0.4320	0.1055	0.5000
O2'	2a	0.5550	0.1309	0.0000	0.5430	0.1337	0.0000
O3'	2a	0.0443	0.3645	0.5000	0.0316	0.3611	0.5000
O4'	2a	0.9054	0.3770	0.0000	0.9012	0.3625	0.0000

TABLE II: Fractional coordinates for  $\text{La}_{0.5}\text{Ca}_{0.5}\text{MnO}_3$  (LCMO) from *ab initio* energy minimization with 100% exact exchange and for  $\text{Pr}_{0.60}\text{Ca}_{0.40}\text{MnO}_3$  (PCMO) from single crystal neutron diffraction [14], both with  $P2_1nm$  symmetry. Wyckoff positions are given in the second column.

Atom	Wyck.	LCMO			PCMO		
		x	y	z	x	y	z
Ca1	2a	0.4769	0.9021	0.0000	0.5121	0.8936	0.0000
La2	2a	0.4783	0.3723	0.5000	0.4784	0.3614	0.5000
La3	2a	0.9832	0.1286	0.0000	0.9977	0.1426	0.0000
Ca4	2a	0.9741	0.6093	0.5000	0.9905	0.6088	0.5000
Mn1	4b	0.0000	0.8743	0.2498	0.0000	0.8756	0.2489
Mn2	4b	0.9611	0.3775	0.7518	0.9795	0.3746	0.7492
O1	4b	0.2717	0.9980	0.2768	0.3044	0.9845	0.2861
O2	4b	0.6918	0.2685	0.7837	0.7090	0.2676	0.7891
O3	4b	0.1818	0.2261	0.7029	0.2112	0.2328	0.7148
O4	4b	0.7324	0.5211	0.2276	0.7515	0.5191	0.2110
O1'	2a	0.4344	0.1246	0.0000	0.4353	0.1125	0.0000
O2'	2a	0.5575	0.1322	0.5000	0.5743	0.1321	0.5000
O3'	2a	0.0375	0.3644	0.0000	0.0562	0.3758	0.0000
O4'	2a	0.9247	0.3777	0.5000	0.9104	0.3846	0.5000

Mn and O ions projected onto the  $\mathbf{ab}$  plane in the  $Pn2_1m$  energy minimized structure. Positions of ions in the ZP CO structure are indicated by shaded or filled circles and positions of ions in the CB CO structure are indicated by dashed lines (Table I). The structures are coincident at the Mn1 ion positions and so this figure facilitates

comparison of distortions in the **ab** plane. The main differences in ion position occur at the Mn2 and O3 positions to accommodate the switch between ZP and CO JT distortion patterns. Transverse wavelike modulations of Mn and O ion positions about ideal perovskite positions can be identified in Fig. 1(a). Modulations of either ion type have wavelength equivalent to the unit cell dimension along the **b** axis and are out of phase by  $\pi/2$  and are similar to modulations of  $\text{MnO}_6$  proposed in manganites with  $x > 0.5$  [5] and  $x < 0.5$  [22].

Positions of ions in the energy minimized  $P2_1nm$  structure with ZP CO are shown in Fig. 1(b). The main differences in atomic positions in the plane between this ZP CO structure and the  $Pn2_1m$  ZP CO structure occur at the O2 and O3 positions. Fractional coordinates for the  $P2_1nm$  structures for both  $\text{La}_{0.5}\text{Ca}_{0.5}\text{MnO}_3$  (this work) and for  $\text{Pr}_{0.60}\text{Ca}_{0.40}\text{MnO}_3$  [14] are compared in Table II and the agreement is remarkable. The starting guess for the  $\text{La}_{0.5}\text{Ca}_{0.5}\text{MnO}_3$  structure in *ab initio* calculations was not the  $\text{Pr}_{0.60}\text{Ca}_{0.40}\text{MnO}_3$  structure and the coordinates obtained via *ab initio* calculations are not simply a relaxation of the  $\text{Pr}_{0.60}\text{Ca}_{0.40}\text{MnO}_3$  structure. There are bonds of intermediate length along the ZP axis ranging from 1.99 to 2.09 Å in *ab initio* calculations and from 1.98 to 2.05 Å in experiment [14] (Table III). Bond valence sums [24] (calculated using  $R_o$  and B values of 1.750 and 0.37 for all Mn-O bonds) for the ZP structures are close to 3.5 in both computed and experimental ZP structures, which is indicative of an intermediate valence. The Mn-O<sup>-</sup>-Mn bond angle is  $160^\circ$  or less in both  $\text{La}_{0.5}\text{Ca}_{0.5}\text{MnO}_3$  and  $\text{Pr}_{0.60}\text{Ca}_{0.40}\text{MnO}_3$ .

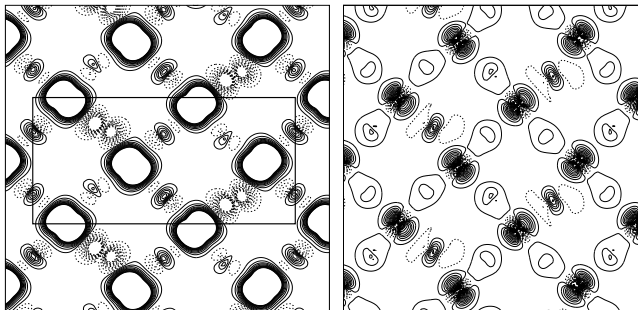


FIG. 2: Spin density and charge density difference for  $\text{La}_{0.5}\text{Ca}_{0.5}\text{MnO}_3$  in the ZP state with A-type magnetic order and  $Pn2_1m$  symmetry obtained using 100% exact exchange. (left) Spin density. The unit cell shown in Fig. 1(a) is outlined. (right) Charge density difference.

The spin density and charge density difference of the ZP CO structure are shown in Fig. 2. Charge density difference plots are generated by subtracting densities of isolated  $\text{O}^{2-}$  and  $\text{Mn}^{4+}$  ions from the total charge density of the crystal structures and therefore show deformations of charge density at O ion sites and  $e_g$  orbital order at Mn ion sites. Each Mn ion in the ZP CO state has a  $d^4$  con-

TABLE III: Selected bond distances in Å, bond angles for LCMO from *ab initio* energy minimization and for PCMO from single crystal neutron diffraction [14] and bond valence sums (BVS). Ion labels refer to atomic positions given in Fig. 1. The bond angle given is the Mn1a-O3a-Mn2 angle at the center of the ZP or adjacent to a JT distorted Mn ion. The structure and space group are indicated at the top of each column.

Bond	CB <sup>a</sup>	ZP <sup>b</sup>	Bond	ZP <sup>c</sup>	ZP <sup>d</sup>
Mn1a-O1a	1.92	1.99	Mn1a-O1a	2.01	2.05
Mn1a-O4	1.86	1.87	Mn1a-O1b	1.86	1.88
Mn1a-O2	1.91	1.89	Mn1a-O2	1.91	1.91
Mn1a-O3a	1.84	2.05	Mn1a-O3a	2.08	1.98
Mn2-O2	1.91	1.89	Mn2a-O2	1.90	1.90
Mn2-O3a	2.14	2.09	Mn2a-O3a	2.09	2.01
Mn2-O1a	1.92	1.86	Mn2a-O4	1.88	1.90
Mn2-O4a	2.15	2.03	Mn2a-O4a	2.02	2.03
Bond angle	160	155		151	159
BVS Mn1	3.28	3.60		3.60	3.5 <sup>d</sup>
BVS Mn2	4.08	3.56		3.53	3.5 <sup>d</sup>

<sup>a</sup> $\text{La}_{0.5}\text{Ca}_{0.5}\text{MnO}_3$   $Pn2_1m$  symmetry, 60% exact exchange

<sup>b</sup> $\text{La}_{0.5}\text{Ca}_{0.5}\text{MnO}_3$   $Pn2_1m$  symmetry, 100% exact exchange

<sup>c</sup> $\text{La}_{0.5}\text{Ca}_{0.5}\text{MnO}_3$   $P2_1nm$  symmetry, 100% exact exchange

<sup>d</sup> $\text{Pr}_{0.60}\text{Ca}_{0.40}\text{MnO}_3$   $P2_1nm$  symmetry, expt. (Ref. [14])

figuration,  $\text{O}^-$  ions order in  $\text{Mn}(d^4)\text{-O}^-\text{-Mn}(d^4)$  dimers (Zener polarons) in **ab** planes and the magnetic ground state is A-type [12]. UHF calculations [12] predict a magnetic moment of  $0.7 \mu_B$  on the  $\text{O}^-$  ion in the center of each ZP, which is opposed to the moments of neighboring ZP Mn ions. On the other hand, cluster configuration interaction (CI) calculations [25] show that the moment on  $\text{O}^-$  ions is much less than  $0.7 \mu_B$ . However they show that the charge on these ions is approximately  $-1.0e$ , in agreement with UHF calculations and that the ZP are strongly bound in a FM state. In both UHF and CI calculations the total magnetic moment on each ZP is  $7/2 \mu_B$  in agreement with experiment [7]. The reason for the discrepancy between spin distributions in CI and UHF calculations is simply that the UHF spin function for the Mn-O<sup>-</sup> bond is  $\alpha\beta$  whereas it should be  $(\alpha\beta - \beta\alpha)/\sqrt{2}$ .  $d_{3x^2-r^2}$  and  $d_{3y^2-r^2}$  orbital order in the ZP state can clearly be seen in Fig. 2 in both spin density and charge density difference plots.

Bond lengths, the Mn1a-O3a-Mn2 bond angle and bond valence sums for the CB state with  $Pn2_1m$  symmetry are given on the left in Table III. Spin densities and charge density differences are given in Fig. 3. The ground state magnetic order for the CB CO state is CE-type, the magnetic order found experimentally in  $\text{La}_{0.5}\text{Ca}_{0.5}\text{MnO}_3$  [2], and it consists of zig-zag FM chains as shown in Fig. 3. Mn1 ions in the chains have short (1.85Å) Mn-O bonds while JT distorted Mn2 ions have long Mn-O bonds (2.15Å). These are, respectively, the

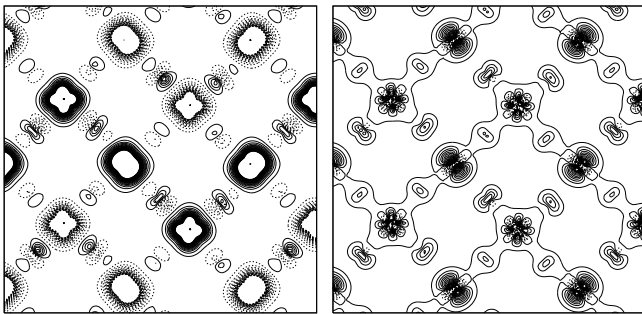


FIG. 3: Spin density and charge density difference for  $\text{La}_{0.5}\text{Ca}_{0.5}\text{MnO}_3$  in the checkerboard state with CE-type magnetic order and  $Pn2_1m$  symmetry obtained using 60% exact exchange. (left) Spin density. (right) Charge density difference.

lengths of Mn-O bonds in  $\text{CaMnO}_3$  and  $\text{LaMnO}_3$  [10, 26]. The magnetic moments on these ions are  $3.23\mu_B$  (Mn1) and  $3.85\mu_B$  (Mn2) and bond valence sums are 3.28 and 4.08. All of these are characteristic of conventional CO, although charges on Mn ions as measured by Mulliken populations are essentially identical, with values of  $+2.02$  (Mn1) and  $+2.02$  (Mn2). A small difference in Mn ion charge has been noted in several experimental papers [15, 16] in apparently CO states.

In summary, we have shown that the equilibrium structure for  $\text{La}_{0.5}\text{Ca}_{0.5}\text{MnO}_3$  which is predicted by hybrid Hartree-Fock/density functional theory depends on the percentage of exact exchange used in the calculation. The CB CO state consists of FM zig-zag chains in which corner (Mn1) ions have short bonds ( $1.85\text{\AA}$ ) while JT distorted (Mn2) ions have long bonds ( $2.15\text{\AA}$ ) to neighboring O ions. A preliminary calculation of the RXD spectrum using this structure is in reasonably good agreement with experimental RXD spectra for  $\text{Pr}_{0.60}\text{Ca}_{0.40}\text{MnO}_3$  [27]. The ZP CO state consists of FM planes tiled with polarons which have Mn-O bonds of intermediate length along the polaron axis and this structure is in reasonable agreement with that found for  $\text{Pr}_{0.60}\text{Ca}_{0.40}\text{MnO}_3$  by neutron scattering [14]. Transformation from the CB to the ZP state requires rehybridization at Mn1 and O3 sites together with relatively minor displacements shown in Fig. 1(a). Effective magnetic moments from magnetic susceptibility data for at least two mixed valence manganites display marked increases in effective magnetic moment on cooling below the CO transition temperature to  $6.1$  [28] or  $7.9\mu_B$  [14]. These magnitudes are similar to the ZP magnetic moment of  $7\mu_B$ . Dimerization of CE zig-zag chains to form a ZP state may produce this large effective moment.

This work was supported by the Irish Higher Education Authority under the PRTLIIITAC2 programme. The author wishes to acknowledge discussions with P.G. Radaelli, A. Daoud-Aladine and S. Grenier.

- 
- [1] C. Chen and S.-W. Cheong, Phys. Rev. Lett. **76**, 4042 (1996).
  - [2] P. G. Radaelli, D. E. Cox, M. Marezio, and S.-W. Cheong, Phys. Rev. B **55**, 3015 (1997).
  - [3] P. G. Radaelli, D. E. Cox, L. Capogna, S.-W. Cheong, and M. Marezio, Phys. Rev. B **59**, 14440 (1999).
  - [4] J. Li, C. Jin, and H. Zhao, Phys. Rev. B **64**, R20405 (2001).
  - [5] T. Nagai, T. Kimura, A. Yamazaki, T. Asaka, K. Kimoto, Y. Tokura, and Y. Matsui, Phys. Rev. B **65**, R60405 (2002).
  - [6] R. Kajimoto, H. Yoshizawa, Y. Tomioka, and Y. Tokura, Phys. Rev. B **66**, R180402 (2002).
  - [7] J. C. Loudon, N. D. Mathur, and P. A. Midgley, Nature **420**, 797 (2002).
  - [8] M. Pissas and G. Kallias, cond-mat/0205410.
  - [9] J. C. Loudon, S. Cox, A. J. Williams, J. P. Attfield, P. B. Littlewood, P. A. Midgley, and N. D. Mathur, cond-mat/0308501.
  - [10] E. O. Wollan and W. C. Koehler, Phys. Rev. **100**, 545 (1955).
  - [11] J. B. Goodenough, Phys. Rev. **100**, 564 (1955).
  - [12] G. Zheng and C. H. Patterson, Phys. Rev. B **67**, 220404(R) (2003).
  - [13] V. Ferrari, M. Towler, and P. Littlewood, Phys. Rev. Lett. **91**, 227202 (2003).
  - [14] A. Daoud-Aladine, J. Rodriguez-Carvajal, L. Pinsard-Gaudart, M. T. Fernandez-Diaz, and A. Revcolevschi, Phys. Rev. Lett. **89**, 97205 (2002).
  - [15] S. Grenier, J. Hill, D. Gibbs, K. Thomas, M. v. Zimmermann, C. Nelson, V. Kiryukhin, Y. Tokura, Y. Tomioka, D. Casa, et al., Phys. Rev. B **69**, 134419 (2004).
  - [16] R. J. Goff and J. P. Attfield, Phys. Rev. B **70**, 140404R (2004).
  - [17] J.-S. Z. F. Rivadulla, E. Winkler and J. Goodenough, Phys. Rev. B **66**, 174432 (2002).
  - [18] G. Subías, J. García, M. Proietti, and J. Blasco, Phys. Rev. B **56**, 8183 (1997).
  - [19] J. García, M. C. Sánchez, G. Subías, and J. Blasco, J. Phys. Condens. Matt. **13**, 3229 (2001).
  - [20] J. García, M. C. Sánchez, J. Blasco, G. Subías, and M. G. Proietti, J. Phys. Condens. Matt. **13**, 3243 (2001).
  - [21] C. Nelson, M. v. Zimmermann, Y. Kim, J. Hill, D. Gibbs, V. Kiryukhin, T. Koo, S.-W. Cheong, D. Casa, B. Keimer, et al., Phys. Rev. B **64**, 174405 (2001).
  - [22] B. Campbell, R. Osborn, D. Argyriou, L. Vasiliu-Doloc, J. Mitchell, S. Sinha, U. Ruett, C. Ling, Z. Islam, and J. Lynn, Phys. Rev. B **65**, 014427 (2001).
  - [23] V. R. Saunders, R. Dovesi, C. Roetti, M. Causá, R. Orlando, C. M. Zicovich-Wilson, N. M. Harrison, K. Doll, B. Civalleri, I. Bush, et al., Crystal03 User's Manual, University of Torino, Torino, 2003. (www.crystal.unito.it).
  - [24] I. D. Brown, Acta Crystallogr. B **48**, 553 (1992).
  - [25] C. H. Patterson, Mol. Phys. (Accepted for publication).
  - [26] J. Rodriguez-Carvajal, M. Hennion, F. Moussa, A. H. Moudden, L. Pinsard, and A. Revcolevschi, Phys. Rev. B **57**, R3189 (1998).
  - [27] S. Grenier, Private communication.
  - [28] A. Prodi, E. Gilioli, A. Gauzzi, F. Licci, M. Marezio,

F. Bolzoni, Q. Huang, A. Santoro, and J. W. Lynn, *Nature Mater.* **3**, 48 (2004).